*Essential Readings in Light Metals: Cast Shop for Aluminum Production.*
Edited by John F. Grandfield and Dmitry G. Eskin.


# 9. HEAT TREATMENT

Modification of the as-cast microstructure is an important step taking place in cast houses. Papers on heat treatment of aluminum alloys are widely covered in other sources than *Light Metals,* however, some very useful papers on the topic have been included here from the Light Metals Cast Shop sessions.

*Essential Readings in Light Metals: Cast Shop for Aluminum Production.*
Edited by John F. Grandfield and Dmitry G. Eskin.



# INVESTIGATING THE ALPHA TRANSFORMATION – A SOLID-STATE PHASE CHANGE OF DISPERSED INTERMETALLIC PARTICLES FROM AN $Al_6$(Fe,Mn) PHASE TO AN α-Al-(Fe,Mn)-Si PHASE

D. T. L. Alexander[1], R. G. Hamerton[2], H. Cama[2] and A. L. Greer[1]

[1]University of Cambridge
Department of Materials Science & Metallurgy
Pembroke Street, Cambridge CB2 3QZ, UK

[2]Alcan International Limited
Banbury Laboratory, Southam Road, Banbury OX16 2SP, UK

## Abstract

Homogenisation of direct chill (DC)-cast AA3104 can beverage stock aluminium alloy causes intermetallic constituent particles to transform from a tetragonal $Al_6$(Fe,Mn) phase to cubic α-Al-(Fe,Mn)-Si phase. Electron microscopy techniques have been used to investigate this transformation in samples of a model Al-0.5Fe-1.0Mn-0.2Si (wt.%) alloy during isothermal heat treatments at 500°C. Elemental mapping using energy-filtered transmission electron microscopy, together with convergent-beam electron diffraction, has revealed that transformation is eutectoid; diffusion of silicon from the aluminium matrix into the $Al_6$(Fe,Mn) particles causes transformation to an α-Al-(Fe,Mn)-Si/aluminium eutectoid. Nucleation appears to be a key factor controlling the overall transformation rate. After transformation, intragranular eutectoid aluminium coalesces and ripens to become intergranular 'Al-spots'. The particle morphologies have been observed by examining deep-etched samples in a FEGSEM. In addition, manganese diffuses into transformed particles, segregating to grain boundaries.

## Introduction

The ability to model the evolution of microstructure through the rolling process stream, from ingot to final product, is becoming increasingly of interest within the aluminium industry. By joining together physically-based microstructural models for the different elements of the process stream, the aim is to be able to predict the formation of solidification microstructure during DC-casting, and its development during subsequent homogenisation and thermo-mechanical processing through hot and cold rolling mills. As a part of this sequence in can body sheet production, a verified mathematical model is required for the 'α-transformation' – a solid-state phase change that occurs during homogenisation of direct-chill cast ingots of AA3104 alloy, when coarse eutectic intermetallic particles transform from a tetragonal $Al_6$(Fe,Mn) phase to a cubic α-Al-(Fe,Mn)-Si phase [1]. It is relevant to beverage can manufacture, owing to an abrading action of the intermetallic particles on tool-pieces during drawing and ironing of can bodies which prevents galling [2,3].

Existing literature examining the α-transformation is inadequate for developing such a model, because underlying rate-controlling processes have not been well identified. For instance, analysis of transformation kinetics by Watanabe [4] suggested that diffusion of manganese through the matrix controlled transformation rate, as the effective activation energy for transformation was similar to that for manganese diffusion. Possible justification for this theory is that manganese must be supplied to the constituent particles for transformation to occur, because there is a higher weight percentage of manganese in α-Al-(Fe,Mn)-Si than in $Al_6$(Fe,Mn) [5]. Yet, although manganese is known to diffuse into the intermetallic constituent particles during heat treatment, there is no connection between the rate of change of manganese content in the constituents and the rate of transformation to α-Al-(Fe,Mn)-Si phase [6]. A similar analysis of transformation rate by Shillington [6] indicated that diffusion of silicon through the aluminium matrix may control transformation rate, yet Cama [7] found that the transformation rate was unchanged by increasing the microsegregation of silicon (hence increasing local solute level of silicon), which implied that diffusion of silicon is not rate-controlling.

Nevertheless, the concentration of free silicon in the aluminium matrix must be a significant factor. Stoichiometric considerations show silicon must be supplied to $Al_6(Fe,Mn)$ for transformation. Increasing the percentage of silicon in the alloy increases the transformation rate and final percentage of α-Al-(Fe,Mn)-Si phase [3,4,7,8]. Moreover, magnesium-free alloys show a greater transformation rate because the lack of formation of $Mg_2Si$ precipitates raises the level of solute silicon in the matrix [4,7].

The composition of AA3104 can body stock alloy is typically Al-0.4Fe-1.0Mn-1.0Mg-0.2Cu-0.12–0.3Si (wt.%) [3]. In addition to the α-transformation, heating of an ingot to a homogenisation temperature of about 600ºC first causes precipitation and then dissolution of $Mg_2Si$ precipitates, followed by precipitation and partial dissolution of α-Al-Mn-Si dispersoids [3,9]. With silicon being involved in all of the above microstructural changes, there is a degree of interaction between them, complicating any investigation into the α-transformation. By conducting our investigation using a magnesium-free Al-0.5Fe-1.0Mn-0.2Si (wt.%) alloy, some of these complications were eliminated because $Mg_2Si$ does not precipitate. This alloy was also chosen because thermodynamic modelling indicated that heat-treatments should produce a reasonable level of transformation to α-Al-(Fe,Mn)-Si phase.

With the aim of producing a more detailed analysis of the kinetics of the α-transformation, we have examined it by focusing on compositional, microstructural and crystallographic changes within the constituent particles. In particular, features of the transformation known as 'Al-spots' have been examined [10]. These are spots of aluminium that have been observed within transformed particles. The investigation has been carried out using a variety of electron microscopy techniques; primarily energy-filtered transmission electron microscopy. By considering the results in relation to data on overall transformation rate for the same samples (collated from microprobe analysis), many details of the transformation have been elucidated.

## Experimental Methods

Superpurity-based bars of Al-0.5Fe-1.0Mn-0.2Si (wt.%) alloy were cast using a direct-chill casting simulator. This apparatus directionally solidifies molten alloy by spraying the base with a jet of cold water, thus simulating the water-cooled solidification of a DC-cast ingot [11]. Sections were taken from the columnar region of solidification in the cast rods, and were then heat-treated isothermally at temperatures of 400ºC, 500ºC and 600ºC. The heat treatments were performed either in a fluidised bed (treatments 1 minute to 2 hours) or in a muffle furnace (15 minutes to 192 hours).

Scanning electron microscopy specimens were made by mounting sections in conducting resin and then grinding and polishing down to a 1 μm diamond finish. Some polished sections were deep etched in NaOH solution. The specimens were examined in an EDX-equipped JEOL 5800LV SEM (working at 10 kV) and a JEOL 6340F FEGSEM (working at 20 kV).

Transmission electron microscopy specimens were made first by mechanically grinding and dimpling 3 mm discs to about 30 μm thickness, and then ion-beam milling at 3.5 kV and an angle of 5° using a Gatan Precision Ion Polishing System (PIPS). Bright-field/dark-field microscopy, selected-area diffraction and convergent-beam electron diffraction (CBED) were carried out in a 300 kV Philips CM30 TEM. Energy-filtered TEM was conducted using a Gatan Image Filter (GIF) equipped 300 kV Philips CM300 FEG(S)TEM. An EMISPEC system on this TEM was also used to take EDX line-scans in a scanning transmission electron microscope mode.

### EFTEM

A GIF consists of an electron-energy-loss spectrometer (EELS) followed by electromagnetic lenses that focus energy-loss electrons on to a charge-coupled device (CCD) camera. Electrons with different energy losses are dispersed in the EELS; an energy-selecting slit then selects electrons with a particular energy loss, and the lenses reform an image out of these electrons. If elastically scattered electrons are selected, a zero-loss (bright-field) image is formed. Elemental maps are made by forming images from characteristic ionisation electron-energy-loss edges. The three-window method and jump-ratio imaging were used to remove background from ionisation edge images. The three-window method uses subtraction of a background calculated by extrapolating from two pre-edge images [12]. This gives quantitative elemental maps, but does not correct for thickness and plural scattering effects. Jump-ratio images are formed by dividing a post-edge image by a pre-edge image. This produces an image that shows variations in composition and that is largely insensitive to thickness variations and diffraction conditions, yet gives only a qualitative indication of elemental distribution [13].

### Electron Microprobe Analysis

"Feature Detect and Classify" (FDC), an automated microprobe analysis technique, was used to quantify phase proportions of constituent particles [7]. A JEOL 733 electron-probe micro-analyser automatically locates and measures the area of particles using a backscattered electron detector, and then determines phase by analysing the chemical composition at the midpoint of the longest chord across each particle. Area fractions (equivalent to volume fractions) are then calculated for each phase. A ratio of (Fe + Mn)/Si is used to discriminate the two phases, using a cut-off value of 23.9. This represents the mid-point between the lowest possible ratio for Al-Fe binary phases and the highest possible ratio for α-Al-(Fe,Mn)-Si phase. The ratio does not include aluminium to prevent it being distorted by inclusion of matrix in the sampling. Around 300 particles were measured in each sample, giving an error in area/volume fraction of about ± 5% – 10%. FDC was carried out on sections cut perpendicular to the growth direction, because this greatly reduced the frequency of duplex (i.e., partially transformed) particles.

## Results

### Morphology of Particles and their Transformation

Figure 1 shows backscattered electron (BE) SEM images of samples annealed for 1 hour and 192 hours at 500ºC. α-Al-(Fe,Mn)-Si phase can be distinguished from $Al_6(Fe,Mn)$, its brighter contrast arising from its higher average atomic number. The images demonstrate that α-Al-(Fe,Mn)-Si grows through the constituent particles; many of the particles are 'duplex', containing both intermetallic phases. Much of the α-Al-(Fe,Mn)-Si contains small spots of aluminium ('Al-spots').

Deep etching was used to investigate the three-dimensional morphology of transformation, as shown in Figures 2a and 2b.

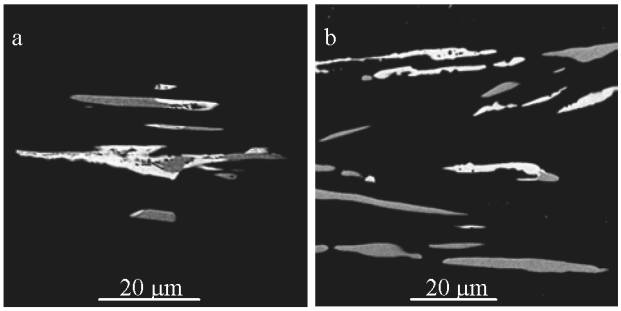


Figure 1: BE SEM images of samples annealed at 500ºC for (a) 1 hour and (b) 192 hours. The α-Al-(Fe,Mn)-Si phase has brighter contrast than $Al_6$(Fe,Mn). Al-spots show as spots of dark contrast within α-Al-(Fe,Mn)-Si phase.

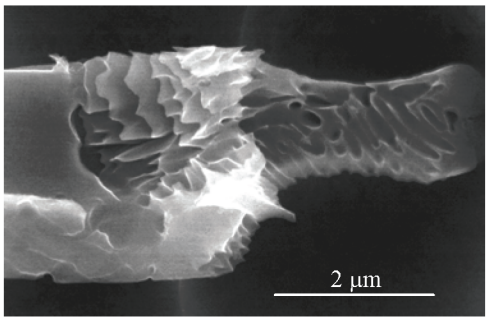


Figure 2a: SE FEGSEM image of a partially transformed particle in alloy annealed for 1 minute at 500ºC. Dissolution of Al-spots has left a laminar structure indicative of eutectoid decomposition.

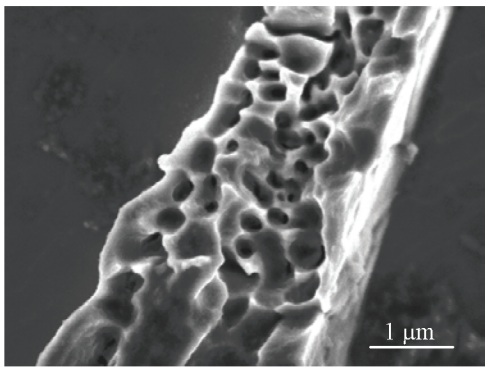


Figure 2b: SE FEGSEM image of a deep-etched α-Al-(Fe,Mn)-Si particle in alloy annealed for 3 hours at 500ºC. Ripening has spheroidised the Al-spots, whose shape is preserved in the etch pits.

The sample in Fig. 2a was made from alloy annealed for 1 minute at 500ºC, and that in Fig. 2b was annealed for 3 hours at 500ºC. Etching dissolved the Al-spots, producing pits and channels in α-Al-(Fe,Mn)-Si phase particles. In contrast, $Al_6$(Fe,Mn) particles would be smooth and monolithic.

Overall Transformation Kinetics

Feature Detect and Classify measurements for isothermal anneals in a muffle furnace at temperatures of 400°C, 500°C and 600°C were used to plot curves of percentage α-Al-(Fe,Mn)-Si phase against time (Fig. 3). Avrami curves of type

$$x = x_f - (x_f - x_0)\exp(-(kt)^n) \qquad (1)$$

have been fitted to the data (where $x$ is the fraction of intermetallic that is α-Al-(Fe,Mn)-Si phase, $x_0$ is the value of $x$ in the as-cast alloy, $x_f$ is the final value of $x$ after a long anneal, $k$ is a temperature dependent rate constant, $t$ is time, $n$ is the Avrami exponent). At 500ºC and 600ºC the curves are not sigmoidal – Avrami exponent $n$ = 1 (note at 600ºC, the curve fitted does not account for the peak in percentage α-Al-(Fe,Mn)-Si phase seen after 2 hours anneal). In contrast at 400ºC the data does have a sigmoidal form, and $n$ = 1.9 for the curve fitted. Two data points are shown for a 6-hour anneal at 400°C; the first measurement (taken using five fields of view spread over 0.5 mm) gave a surprisingly high percentage α-Al-(Fe,Mn)-Si phase (67%). The second measurement, taken on the same specimen, gave a percentage of α-Al-(Fe,Mn)-Si (45%) more consistent with the other specimens. This difference may have been due to variations in local composition.

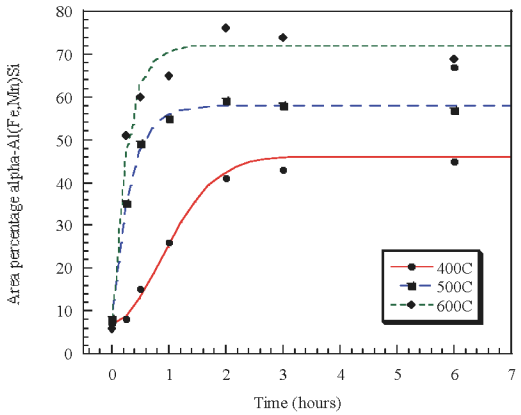


Figure 3: Shows degree of transformation over time. Avrami curves have been fitted to the data, with exponents $n$ = 1 at 500ºC and 600ºC, and $n$ = 1.9 at 400ºC.

Compositional Studies

Figure 4 shows zero-loss bright-field and elemental jump-ratio energy-filtered images of a transformed particle in a specimen made from alloy heat-treated for 2 minutes at 500ºC. There are Al-spots within the grain of α-Al-(Fe,Mn)-Si – i.e. 'intragranular' Al-spots. There is a higher concentration of manganese around the perimeter of the particle, due to diffusion of manganese into the particle from the matrix. A silicon jump-ratio image shows that the concentration of silicon across the particle is uniform; silicon was undetectable in the matrix (detection limit ~ 1 at.%).

Figure 5 shows an α-Al-(Fe,Mn)-Si particle in a sample heat-treated for 15 minutes at 500ºC. The particle contains five grains of α-Al-(Fe,Mn)-Si phase; there are some Al-spots between the grains – i.e. 'intergranular' Al-spots. Again, there is evidence of manganese diffusion around the particle perimeter, and down some grain boundaries (where there is also depletion of iron).

Figure 6 shows a multi-grain α-Al-(Fe,Mn)-Si phase particle in a sample heat-treated for 192 hours at 500°C. Grain boundaries show strong concentration of manganese and depletion of iron Figure 7 shows an untransformed $Al_6$(Fe,Mn) particle from the same specimen. There has been phase separation into an iron-rich region and a manganese-rich region.

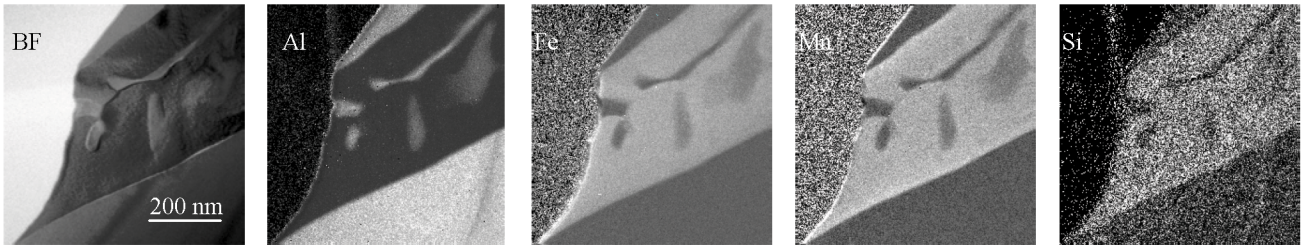


Figure 4: Zero-loss bright-field and jump-ratio energy-filtered TEM images of a transformed particle in alloy annealed for 2 minutes at 500ºC. Transformation has produced Al-spots *within* the grain of α-Al-(Fe,Mn)-Si – i.e. 'intragranular' Al-spots. Silicon is present at a constant level throughout the α-Al-(Fe,Mn)-Si phase, and the concentration of manganese is increased along the particle/matrix interface.

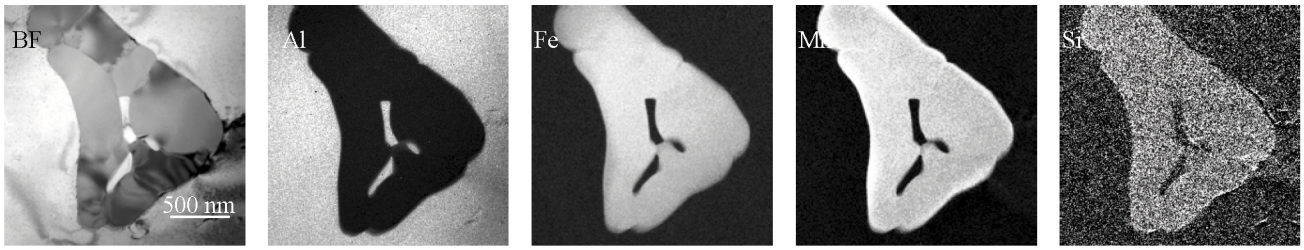


Figure 5: Zero-loss bright-field and jump-ratio TEM energy-filtered images of a multi-grain α-Al-(Fe,Mn)-Si particle in alloy annealed for 15 minutes at 500ºC. There are *intergranular* Al-spots in the centre of the particle. Manganese has continued to diffuse into the particle, and has started diffusing down grain boundaries.

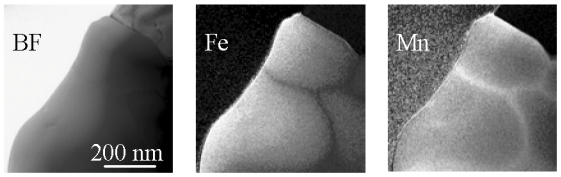


Figure 6: Energy-filtered TEM images of an α-Al-(Fe,Mn)-Si particle in alloy annealed for 192 hours at 500ºC. Segregation of manganese to α-Al-(Fe,Mn)-Si grain boundaries has been matched by depletion of iron.

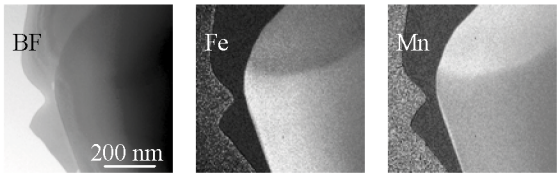


Figure 7: Energy-filtered TEM images of an $Al_6(Fe,Mn)$ particle in alloy annealed for 192 hours at 500ºC. Diffusion of manganese into the particle has been followed by phase separation into a manganese-rich phase and an iron-rich phase.

## Discussion

### Eutectoid Transformation

A detailed microstructural investigation was made of samples annealed for just 1 or 2 minutes at 500ºC. The annealing produced low levels of transformation overall, yet induced transformation in some particles. Using TEM, it was observed that the transformed particles all contained a mixture of α-Al-(Fe,Mn)-Si and intragranular Al-spots (e.g. see Fig. 4), indicating that transformation of $Al_6(Fe,Mn)$ is eutectoid: silicon diffuses into $Al_6(Fe,Mn)$ from the matrix, pushing the composition of the particle across a phase boundary into a two-phase field of α-Al-(Fe,Mn)-Si and aluminium. Assuming the volume of the constituent particle remains constant during transformation, volumetric considerations determine the stoichiometry of the α-Al-(Fe,Mn)-Si phase, (with aluminium atoms substituting for silicon atoms [14]). Thus the stoichiometry of transformation is:

$$3Al_6(Fe,Mn) + Si \rightarrow \alpha\text{-}Al_{12}(Fe,Mn)_3Si + 6Al \qquad (2)$$

This would produce a eutectoid that is about 75% α-Al-(Fe,Mn)-Si phase and 25% aluminium – in qualitative agreement with observations. Examination of samples using other techniques supports the conclusion that transformation is eutectoid. Dissolution of Al-spots in transformed particles leaves plate-like skeletal intermetallic structures, indicating that transformation had produced the two-phase lamellar intergrowth expected from eutectoid decomposition (Fig. 2a). CBED has been used to compare the crystallographic orientations of intragranular Al-spots to the orientation of aluminium matrix surrounding a particle. The Al-spots were found to have a near-identical orientation, perhaps as a result of branching during eutectoid growth, and this orientation differed from the matrix, showing that they had grown independent of the matrix.

The eutectoid nature of the α-transformation results in a decrease in volume of intermetallic phase, thus increasing the concentration of iron and manganese. Therefore diffusion of manganese into constituents is not necessary for the transformation.

### Diffusion of Silicon

Since diffusion of silicon from the matrix into the constituent particles is necessary for transformation, it was expected that transformed particles would exhibit diffusion gradients of silicon from the particle/matrix interfaces, and that silicon would be seen diffusing into some $Al_6(Fe,Mn)$ particles prior to transformation.

Neither of these results was found; the concentration of silicon across transformed particles was always constant (e.g. see Figs 4 - 6), and silicon was never present in untransformed particles. This could be due to silicon supplying the transformation by diffusing down grain boundaries between $Al_6(Fe,Mn)$ and the growing α-Al-(Fe,Mn)-Si phase. A simple estimate shows that diffusion of silicon through aluminium may control the growth rate of α-Al-(Fe,Mn)-Si in a particle: assuming silicon supplies the transformation from the dispersoid-free zone around the constituents (about 5 μm in width), at 500°C transformation would occur in around 180 s ($D_{Si} \sim 1.4 \times 10^{-13}$ $m^2$ $s^{-1}$ [15]) – a time scale of the same order as that observed. SEM images show that transformation proceeds from separate nuclei on particle/matrix interfaces. After nucleation, particles do not always completely transform, with duplex particles observed in samples given anneals in excess of the time needed for the α-transformation to finish. This incomplete transformation is due to localised depletion of silicon in the matrix surrounding the particles.

Ripening of Al-spots

After transformation of a particle, Al-spots evolve, ripening to decrease surface energy. Intragranular aluminium diffuses to α-Al-(Fe,Mn)-Si grain boundaries, forming intergranular Al-spots (see Fig. 5). As with intragranular Al-spots, CBED analysis found that the crystallographic orientation of intergranular Al-spots differs from the matrix. Eutectoid aluminium also diffuses to the matrix, hence intergranular Al-spots are typically located in the centre of multi-grain particles – in accordance with observations made by Trømborg [10]. TEM examination has shown that ripening is considerably faster at 600°C, with intergranular Al-spots seen after just 1 minute of heat-treatment.

In addition to coarsening, Al-spots spheroidise to decrease surface energy, as seen in a deep-etched sample of alloy annealed for 3 hours at 500°C. Comparison of BE SEM images of alloys annealed for 1 hour and 192 hours at 500°C also demonstrates ripening (Fig. 1); not only have the Al-spots spheroidised after 192 hours heat-treatment, the overall volume of intraparticle aluminium has decreased due to continuing diffusion of eutectoid aluminium into the matrix.

Transformation Rate

The curves of percentage α-Al-(Fe,Mn)-Si phase against annealing time at 500°C and 600°C (Fig. 3) conform to a curve of

$$x = x_f - (x_f - x_0)\exp(-kt) \qquad (3)$$

rather than the sigmoidal curve typical of solid-state transformations. Microstructural investigations (using TEM) of samples annealed at 500°C show that this is due to nucleation controlling the transformation rate. Firstly, the growth rate of α-Al-(Fe,Mn)-Si through a particle is fast relative to the overall transformation rate of the system of particles. Secondly, whereas transformed particles in samples heat-treated for 1 or 2 minutes contain only intragranular Al-spots, a mixture of intragranular and intergranular Al-spots is seen in samples heat-treated for 15 minutes and 3 hours. This indicates that transformation had nucleated after different times so ripening was interrupted at different stages. Ripening of Al-spots could be the origin of the peak in percentage α-Al-(Fe,Mn)-Si phase seen after 2 hours anneal at 600°C; when the Al-spots are small, FDC may include them in particle areas. After they have ripened, FDC is more likely to resolve them, so they would not then be included in particle areas and therefore the measured area of α-Al-(Fe,Mn)-Si phase would decrease despite there being no changes in volume fraction.

In contrast to the transformation curves at 500°C and 600°C, that for 400°C is sigmoidal, because of an initially low transformation rate. This suggests that growth of α-Al-(Fe,Mn)-Si is now sufficiently slow to affect overall transformation rate. At 400°C, the diffusion coefficient of silicon in aluminium is $\sim 5.8 \times 10^{-15}$ $m^2s^{-1}$ [15]. Again supposing transformation is enabled by silicon diffusing from a precipitate-free zone of 5 μm, transformation of a particle is estimated to take about 70 minutes. Therefore the growth rate would be an order of magnitude slower than at 500°C, and would produce a 'toe' region in the transformation curve. Transformation rate is observed to increase as annealing temperature is raised. This is because atomic mobility is greater, which will increase the nucleation rate of the α-Al-(Fe,Mn)-Si phase.

Manganese Diffusion

FDC measurements show that the average Fe/Mn ratio decreases during heat-treatment for both intermetallic phases (see Table I). This accords with the results of Watanabe [4], Shillington [6] and Rouns [9]. Because iron has very low solid solubility in aluminium (≤ 0.04% [16]), these changes are due to diffusion of manganese into the particles. At 400°C the effect is not strong; also the final Fe/Mn ratio for α-Al-(Fe,Mn)-Si is, at 1.6, greater than the initial ratio for $Al_6(Fe,Mn)$. Since the ratio should not change during eutectoid transformation, this appears to show that manganese diffuses *out* of the transformed particles, but is actually because of two other factors. Partly, it is a result of the influence of as-cast α-Al-(Fe,Mn)-Si phase particles on measurement statistics (these having a greater average Fe/Mn ratio than $Al_6(Fe,Mn)$); analysis of the data has revealed it is also because there is preferential transformation of $Al_6(Fe,Mn)$ particles that have a higher than average Fe/Mn ratio (e.g. Fe/Mn > 2). At 600°C, diffusion of manganese into the particles caused significant particle growth, the overall volume percent of constituent increasing by about 50%. This did not occur at 500°C because the volume of dispersoids is much greater, decreasing the amount of manganese and silicon available for growth.

Table I Fe/Mn ratios for as-cast and annealed alloy

| Alloy | $Al_6(Fe,Mn)$ | α-Al-(Fe,Mn)-Si |
|---|---|---|
| As-cast | 1.4 | 2.7 |
| 192 hours at 400°C | 1.2 | 1.6 |
| 192 hours at 500°C | 0.9 | 1.0 |
| 192 hours at 600°C | 0.9 | 0.9 |

The diffusional process can be observed in energy-filtered images of α-Al-(Fe,Mn)-Si particles in samples annealed at 500°C. Initially the concentration of manganese increases around the particle perimeter (Fig. 4); subsequently, manganese starts diffusing down α-Al-(Fe,Mn)-Si grain boundaries (Fig. 5). Continued development leads to heavy concentration of manganese at the grain boundaries after 192 hours heat-treatment,

with iron concentrated in the centre of the particles (Fig. 6). These changes occur at a much slower rate than growth of α-Al-(Fe,Mn)-Si, probably because the diffusion coefficient of manganese in aluminium, at ~ $1 \times 10^{-16}$ $m^2$ $s^{-1}$ at 500°C [15], is significantly lower than for silicon.

Diffusion of manganese into $Al_6$(Fe,Mn) produces different compositional variations when compared to the grain-boundary segregation in α-Al-(Fe,Mn)-Si phase. Figure 7 shows energy-filtered images of an $Al_6$(Fe,Mn) particle in a sample heat-treated for 192 hours. There has been phase separation into an iron-rich phase and a manganese-rich phase. Selected-area diffraction patterns of the two regions showed that, although they were epitaxial, the unit-cell dimensions of the manganese-rich phase were larger than for the iron-rich phase – showing the same trend as the difference in cell dimensions of $Al_6Mn$ and $Al_6Fe$.

## Conclusions

By combining information from microstructural investigation of transformation within particles with the analysis of overall transformation rates during isothermal anneals, many aspects of the α-transformation can now be understood. Although diffusion of silicon from the matrix into the intermetallic particles controls growth of the α-Al-(Fe,Mn)-Si phase, the growth rate is fast relative to the nucleation rate at annealing temperatures of 500°C and 600°C. As a result, the transformation rate is nucleation-controlled at those temperatures. At 400°C, there is evidence that growth rate is significantly slower than at 500°C and 600°C, leading to a sigmoidal curve of transformation against time with an initial region of low transformation rate.

Because the α-transformation is eutectoid, the transformation does not require diffusion of manganese into the intermetallic particles even though α-Al-(Fe,Mn)-Si has a higher concentration of transition metal than $Al_6$(Fe,Mn). Despite this, manganese does diffuse into both phases during heat-treatments, yet this is not thought to affect the transformation. At 600°C, it does result in considerable growth of the constituent particles. At 500°C manganese would concentrate on grain boundaries in α-Al-(Fe,Mn)-Si phase, yet a phase separation into discrete regions of manganese-rich phase and iron-rich phase are observed in $Al_6$(Fe,Mn).

## Acknowledgments

DTLA is supported by an Engineering & Physical Sciences Research Council CASE studentship, in conjunction with Alcan International Limited. The authors thank P.J. Thomas, P.A. Midgley, D.A. Nicol, D. Vowles and M. Weyland for help with microscopy. They also thank A. Bosland for making the FDC measurements and J. Worth for preparing the alloy rods.

## References

1. P. Furrer, "Structural Changes During Heat-Treatment of Direct Chill-Cast Al-Mn Alloy," Z. Metallk. 70 (1979), 699.

2. W. F. Hosford and J. L. Duncan, "The Aluminum Beverage Can," Scientific American September (1994) 34.

3. E. J. Westerman, "Silicon: A Vital Alloying Element in Aluminum Beverage Can Body Stock," Aluminum Alloys for Packaging, ed. J. G. Morris et al. (Warrendale, PA: The Minerals, Metals & Materials Society, 1993), 1.

4. H. Watanabe, K. Ohori and Y. Takeuchi, "Phase Change in 3004 Base Alloys at Elevated Temperatures," Aluminium 60 (1984), 310.

5. T. C. Sun, "The Effect of Preheating on AA3104 Aluminum Alloy Ingot Structure and Particulate Composition," Aluminum Alloys for Packaging, ed. J. G. Morris et al. (Warrendale, PA: The Minerals, Metals & Materials Society, 1993), 31.

6. E. Shillington, "Thermal Stability of Metastable Intermetallic Phases in Model Al-Fe and Al-Fe-Mn-Si Alloys" (Part II Thesis, Oxford University, 1996).

7. H. Cama et al., "Intermetallic Phase Selection and Transformation in Aluminium 3xxx Alloys," SP'97 Proceedings of the 4th Decennial International Conference on Solidification Processing, ed. J. Beech and H. Jones, (London: The Institute of Metals, 1997), 555.

8. P. N. Anyalabechi, T. N. Rouns and R. E. Sanders, "Microstructural Analysis of Second Phases Developed During Casting and Preheating of 3XXX Aluminum Alloys," (Paper presented at RASELM, Conference on Science and Engineering of Light Metals, Sendai, Japan, 1991) 923.

9. T. N. Rouns, "Composition and Preheating Effects on Dispersoid and Insoluble Constituent Particle Evolution in 3XXX Alloys," Aluminum Alloys for Packaging III, ed. S. K. Das (Warrendale, PA: The Minerals, Metals & Materials Society, 1998), 3.

10. E. Trømborg, A. L. Dons and L. Arnberg, "Investigation of the $Al_6$(Mn,Fe) → α-Al(Mn,Fe)Si Phase Transformation During Homogenization of AA3003 and AA3004 Aluminium Alloys," Aluminium Alloys: their Physical and Mechanical Properties: ICAA3 ed. L. Arnberg et al. (Trondheim: SINTEF Metallurgy, 1992) 270.

11. S. J. Maggs et al., "The Effect of Trace Elements on Intermetallic Phase Selection in Simulated DC Casting," Light Metals 1995, (Warrendale, PA: The Minerals, Metals & Materials Society 1995) 1039.

12. P. A. Crozier, "Quantitative Elemental Mapping of Materials by Energy-Filtered Imaging," Ultramicroscopy 58 (1995), 157.

13. F. Hofer, P. Warbichler and W. Grogger, "Imaging of Nanometer-Sized Precipitates in Solids by Electron Spectroscopic Imaging," Ultramicroscopy 59 (1995), 15.

14. A. L. Dons, "Superstructures in α-Al(Mn,Fe,Cr)Si," Z. Metallk. 76 (1985), 151.

15. E. A. Brandes and G. B. Brook, ed., Smithells Metals Reference Book 7th Edition (Oxford: Butterworth-Heinemann Ltd., 1992) 13-16.

16. J. E. Hatch, Aluminum Properties and Physical Metallurgy (USA, American Society for Metals, 1990), 230.